

Exhaustive Circuit Mapping of a Single-Cell Foundation Model Reveals Massive Redundancy, Heavy-Tailed Hub Architecture, and Layer-Dependent Differentiation Control

Ihor Kendiukhov

Department of Computer Science, University of Tübingen, Germany

kendiukhov@gmail.com

Abstract

Mechanistic interpretability of biological foundation models has relied on selective feature sampling, pairwise interaction testing, and observational trajectory analysis—each introducing systematic biases. Here we present three experiments that address these limitations through exhaustive circuit tracing, higher-order combinatorial ablation, and causal trajectory steering in Geneformer, a transformer-based single-cell foundation model. First, exhaustive tracing of all 4,065 active sparse autoencoder features at layer 5 yields 1,393,850 significant downstream edges—a 27-fold expansion over selective sampling—revealing a heavy-tailed hub distribution where 1.8% of features account for disproportionate connectivity and 40% of the top-20 hubs lack biological annotation, demonstrating systematic annotation bias in prior selective analyses. Second, three-way combinatorial ablation across 8 feature triplets shows that redundancy deepens monotonically with interaction order (three-way ratio 0.59 vs. pairwise 0.74) with zero synergy, confirming that the model’s circuit architecture is fundamentally subadditive at all tested orders. Third, trajectory-guided feature steering establishes a causal link between layer position and differentiation directionality: late-layer features (L17) universally push cell states toward maturity (fraction positive = 1.0), while early- and mid-layer features (L0, L11) predominantly push away from maturity (fraction positive = 0.00–0.58), transitioning from correlation to causal evidence for layer-dependent cell state control.

1 Introduction

Single-cell foundation models such as Geneformer [Theodoris et al., 2023], scGPT [Cui et al., 2024], scBERT [Yang et al., 2022], and scFoundation [Hao et al., 2024] learn rich representations of cellular state from large-scale transcriptomic data [Regev et al., 2017, Zheng et al., 2017]. Built on the transformer architecture [Vaswani et al., 2017, Devlin et al., 2019], these models encode genes as tokens in a high-dimensional residual stream [He et al., 2016, Elhage et al., 2022], where biological information is distributed across many dimensions in superposition [Elhage et al., 2022]. Recent work in mechanistic interpretability [Bereska and Gavves, 2024, Olah et al., 2020] has applied sparse autoencoders (SAEs) [Cunningham et al., 2023, Bricken et al., 2023, Gao et al., 2024, Sharkey et al., 2022] to decompose these representations into interpretable biological features [Kendiukhov, 2025b], traced causal circuits between them [Kendiukhov, 2025a], and identified sparse feature circuits [Marks et al., 2024, Conmy et al., 2023]. A companion study demonstrated that attention-based interpretability captures co-expression rather than causal regulation [Kendiukhov, 2025c]. However, these analyses were constrained by three systematic limitations.

First, *annotation bias*: only 30 features per layer were traced, selected from the most biologically annotated features. This sampling strategy systematically excluded unannotated features that may serve critical computational roles. Second, *pairwise-only interactions*: combinatorial ablation tested only pairs of features, leaving open whether higher-order interactions—synergy or deeper redundancy—emerge at third or higher orders. Third, *observational trajectory dynamics*: the discovery that certain features track differentiation trajectories [Trapnell et al., 2014, Wolf et al., 2019] was correlational, lacking causal evidence that amplifying these features would directionally shift cell state.

This paper addresses all three limitations. We report exhaustive circuit tracing of every active feature at a single layer, revealing the complete computational graph for the first time. We extend combinatorial ablation to three-way interactions, testing whether redundancy deepens or synergistic logic gates emerge. And we perform trajectory-guided feature steering—drawing on activation steering and representation engineering methods developed for language models [Turner et al., 2023, Li et al., 2024, Zou et al., 2023]—to causally test whether layer position determines the directionality of cell state change.

Our results reveal a circuit architecture characterized by massive redundancy, heavy-tailed connectivity, systematic annotation bias in prior selective analyses, and a striking layer-dependent gradient in which late-layer features causally push cells toward maturity while early-layer features push them away. These findings transform our understanding of how biological foundation models organize and process cellular information.

2 Results

2.1 Exhaustive circuit tracing reveals the complete L5 computational graph

To eliminate annotation bias, we traced all 4,065 features at layer 5 that met a minimum activation frequency threshold (≥ 0.001), measuring their causal downstream effects on SAE features at layers 6, 11, and 17 across 20 K562 cells [Replogle et al., 2022]. This approach follows the causal mediation framework [Vig et al., 2020, Geiger et al., 2021, Meng et al., 2022]: for each source feature, we ablated its SAE activation (setting it to zero in the residual stream) and measured the resulting Cohen’s d effect size on every downstream feature using Welford’s online algorithm [Welford, 1962], retaining edges exceeding $|d| > 0.5$ with consistency > 0.7 [Cohen, 1988].

This exhaustive analysis produced 1,393,850 significant edges—a 27-fold expansion over the 52,116 edges obtained from selective tracing of 30 features in our companion study [Kendiukhov, 2025a]. The mean number of edges per feature was 342.9 (median 284, range 0–2,138), with 8 features having zero significant edges (Table 1).

2.1.1 Heavy-tailed hub distribution

The edge count distribution is strongly right-skewed (Figure 1A), with 72 features (1.8%) having more than 1,000 edges and 759 features (18.7%) exceeding 500 edges. This heavy-tailed distribution is reminiscent of scale-free network architectures [Barabási and Albert, 1999, Albert and Barabási, 2002, Barabási and Oltvai, 2004], where hub nodes are disproportionately important for network function [Jeong et al., 2001]. This suggests that a small number of hub features serve as major computational bottlenecks through which information must flow.

The top hub feature was F898 (Negative Regulation of Gene Expression, GO:0010629) with 2,138 edges, followed by F1762 (G2/M Transition of Mitotic Cell Cycle, GO:0000086 [Malumbres and Barbacid, 2009]) with 2,098 edges (Table 2).

Table 1: Comparison of selective and exhaustive circuit tracing at layer 5.

Metric	Selective tracing	Exhaustive tracing
Features traced	30	4,065
Total edges	52,116	1,393,850
Mean edges/feature	1,737	343
Median edges/feature	—	284
Max edges	—	2,138
Features with 0 edges	—	8
Cells per feature	200	20
Downstream layers	12	3
Compute time	7.5 hr	17.7 hr

2.1.2 Signal attenuation across layers

Causal effects attenuate monotonically with distance from the source layer: L6 received 694,646 significant edges (49.8%), L11 received 443,381 (31.8%), and L17 received 255,823 (18.4%) (Figure 1C). This 2.7-fold attenuation from L6 to L17 is consistent with the attenuation patterns observed in selective tracing [Kendiukhov, 2025a] and reflects the progressive dilution of single-feature perturbations across intervening computational layers.

2.1.3 Annotation bias in selective tracing

A striking finding is that 8 of the top-20 hub features (40%) are unannotated—they lack any biological pathway annotation from GO [Ashburner et al., 2000], KEGG [Kanehisa and Goto, 2000], or Reactome [Jassal et al., 2020] databases (Table 2, Figure 2). This contrasts sharply with the overall annotation rate of 53.8% across all 4,065 features, meaning that computational importance and biological annotation are not well correlated. The selective tracing approach used in prior work, which required biological annotation for feature selection, would have systematically missed these computationally central but biologically uncharacterized features.

This reveals a fundamental methodological concern for interpretability studies: selecting features based on annotation status introduces a bias toward well-characterized biology, potentially missing the most computationally important features in the network. The annotation enrichment analysis (Figure 2C) shows that the fraction of annotated features among the top-100 and top-20 hubs does not significantly exceed the baseline rate, confirming that annotation status is not predictive of computational centrality.

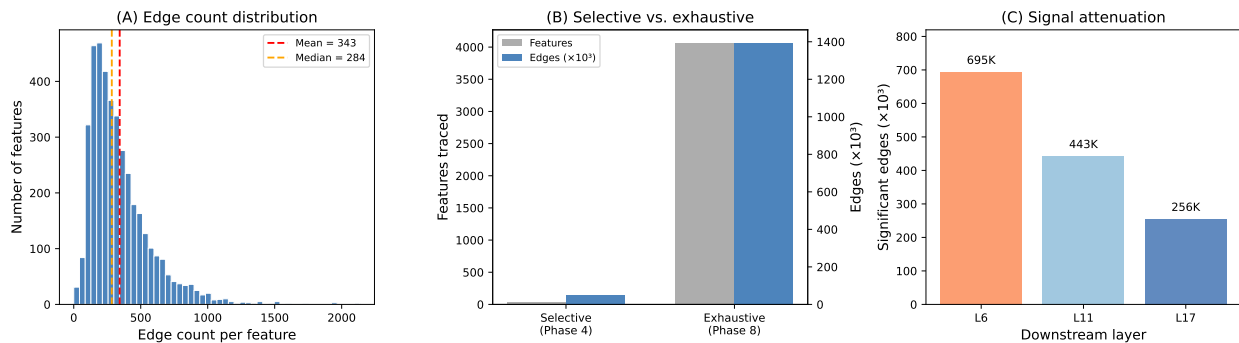


Figure 1: **Exhaustive L5 circuit map overview.** (A) Distribution of edge counts across all 4,065 features, showing heavy-tailed distribution with mean 343 and median 284. (B) Comparison of selective (30 features, 52K edges) versus exhaustive (4,065 features, 1.39M edges) tracing. (C) Signal attenuation across downstream layers: L6 (695K) \rightarrow L11 (443K) \rightarrow L17 (256K).

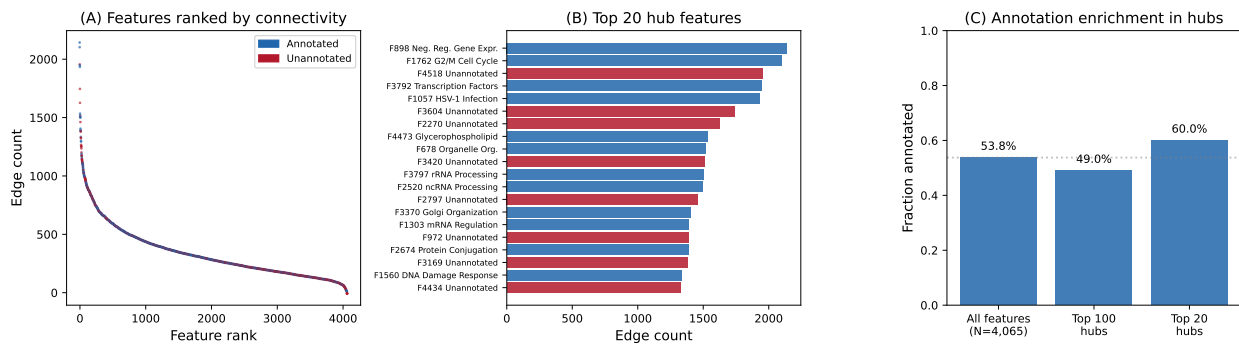


Figure 2: **Hub architecture and annotation bias.** (A) Features ranked by edge count, colored by annotation status (blue = annotated, red = unannotated). (B) Top 20 hub features with edge counts, colored by annotation status. (C) Fraction of annotated features among all features, top 100, and top 20, showing no enrichment for annotation in hubs.

2.2 Higher-order ablation confirms redundancy deepens with interaction order

Our companion study [Kendiukhov, 2025a] established that pairwise combinatorial ablation of same-pathway features produces universally subadditive effects (median redundancy ratio 0.74), with zero synergy across 20 feature pairs. A natural question is whether this pattern extends to higher-order interactions: does ablating three related features simultaneously reveal emergent synergy, or does redundancy continue to deepen?

We tested 8 feature triplets across 4 biological pathways (vesicle transport, mitosis [Malumbres and Barbacid, 2009, Musacchio and Salmon, 2007], metabolism [Chandel, 2021, Simons and Ikonen, 2000], and a cross-pathway DDR [Ciccia and Elledge, 2010, Jackson and Bartek, 2009] \times mitosis combination), measuring the effects of all 7 ablation combinations (A, B, C, AB, AC, BC, ABC) on downstream L17 SAE features across 200 K562 cells each.

Table 2: Top 20 hub features at layer 5 ranked by total edge count. Annotation status indicates whether the feature has a biological pathway annotation.

Rank	Feature	Total edges	Annotation
1	F898	2,138	Neg. Reg. Gene Expression
2	F1762	2,098	G2/M Transition
3	F4518	1,951	<i>unannotated</i>
4	F3792	1,943	Transcription factors
5	F1057	1,930	Herpes simplex infection
6	F3604	1,743	<i>unannotated</i>
7	F2270	1,624	<i>unannotated</i>
8	F4473	1,532	Glycerophospholipid Biosyn.
9	F678	1,516	Organelle Organization
10	F3420	1,508	<i>unannotated</i>
11	F3797	1,500	rRNA Processing
12	F2520	1,499	ncRNA Processing
13	F2797	1,460	<i>unannotated</i>
14	F3370	1,404	Golgi Organization
15	F1303	1,387	Reg. mRNA Metabolism
16	F972	1,386	<i>unannotated</i>
17	F2674	1,386	Protein Modification
18	F3169	1,378	<i>unannotated</i>
19	F1560	1,334	DNA Damage Response
20	F4434	1,327	<i>unannotated</i>

2.2.1 Redundancy deepens monotonically

The three-way redundancy ratio—the fraction of the combined ABC effect that would be expected from the sum of individual effects—was 0.59 for same-pathway triplets and 0.56 for the cross-pathway triplet (Table 3). Both are substantially below the pairwise ratio of 0.74, confirming that redundancy deepens monotonically with interaction order (Figure 3A).

The marginal contribution of the third feature given that the first two are already ablated ($C|AB$) was near zero for most triplets (median range 0.006–0.183), indicating that two features from the same pathway already capture most of the unique information, and a third adds negligible additional disruption.

2.2.2 Zero synergy persists at third order

Across all 8 triplets and 5,000 target-feature instances with at least one significant effect, superadditive (synergistic) effects were observed for only 7 instances (0.14%), compared to 4,703 subadditive instances (94.1%) and 290 additive instances (5.8%). This extends the zero-synergy finding from pairwise to three-way interactions: the model’s circuit architecture contains no higher-order logical gates that require the simultaneous presence of multiple pathway features to activate.

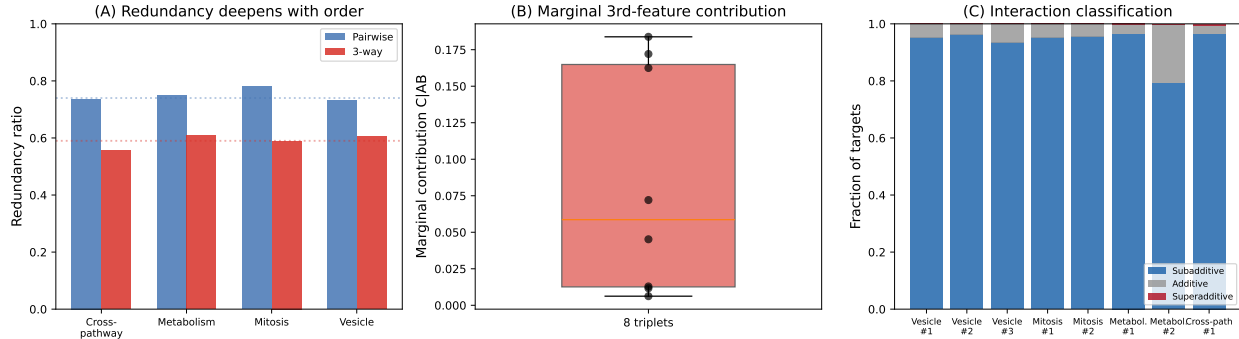


Figure 3: **Redundancy deepens with interaction order.** (A) Grouped bars comparing mean pairwise ratio (0.74) and three-way ratio (0.59) across pathways. (B) Box plot of marginal third-feature contribution $C|AB$, showing near-zero values for most triplets. (C) Stacked bars showing the fraction of subadditive, additive, and superadditive targets per triplet—subadditivity dominates universally.

Table 3: Three-way ablation results for 8 feature triplets. Pairwise ratios are averaged over the three pairs within each triplet. Marginal $C|AB$ reports the median contribution of the third feature given the first two are ablated.

Pathway	Type	Pairwise ratio	3-way ratio	Super. count	Marginal $C AB$
Vesicle	Same	0.73	0.607	0	0.072
Vesicle	Same	0.72	0.593	0	0.045
Vesicle	Same	0.74	0.619	0	0.013
Mitosis	Same	0.78	0.585	0	0.184
Mitosis	Same	0.78	0.594	0	0.162
Metabolism	Same	0.73	0.548	2	0.006
Metabolism	Same	0.77	0.669	1	0.012
DDR×Mitosis	Cross	0.74	0.556	4	0.172
Mean (same)		0.75	0.594	0.4	0.071
Cross-pathway		0.74	0.556	4	0.172

2.3 Trajectory-guided feature steering reveals layer-dependent directionality

Our companion study [Kendiukhov, 2025a] identified 14 “switch features” across layers 0, 5, 11, and 17 whose activation patterns track immune cell differentiation in Tabula Sapiens [The Tabula Sapiens Consortium, 2022] tissue. All 14 were ON-switches (higher activation in mature cells), but this association was purely observational—it could not distinguish whether these features *encode* differentiation signals or merely correlate with them.

To establish causality, we performed trajectory-guided feature steering: for each switch feature, we amplified its SAE activation by factors $\alpha = 2$ and $\alpha = 5$ in early-pseudotime cells [Haghverdi et al., 2016] and measured whether the resulting logit changes shifted cell state toward maturity (positive shift) or away from maturity (negative shift). The state shift metric was computed as the change in cosine similarity between the cell’s logit vector and gene signatures characteristic of late-pseudotime versus early-pseudotime cells.

2.3.1 Layer position determines steering directionality

The most striking finding is that layer position is a near-perfect predictor of steering directionality (Figure 4):

- **L17 features** (3/3 tested) produced positive state shifts in 100% of steered cells (fraction positive = 1.0), consistently pushing early cells toward maturity.
- **L0 features** (5/5 tested) produced negative or mixed shifts (fraction positive = 0.08–0.58), predominantly pushing cells *away* from maturity.
- **L5 features** (2/2 tested) showed mixed behavior (fraction positive = 0.43–0.91).
- **L11 features** (4/4 tested) predominantly pushed cells away from maturity (fraction positive = 0.00–0.44, mean 0.26).

This layer-dependent gradient—from progenitor maintenance at L0 to maturation drive at L17—transforms the observational finding of differentiation-tracking features into causal evidence that layer position encodes the *direction* of cell state change (Figure 6C).

2.3.2 Effect sizes are small but directionally consistent

The absolute magnitude of state shifts was small (mean $|\Delta| \approx 0.001$ – 0.003 at $\alpha = 5$), reflecting the modest impact of amplifying a single feature among $\sim 4,600$ in an overcomplete representation. However, the directionality was remarkably consistent: L17 features achieved perfect positive fraction (1.0) despite the tiny absolute shifts, suggesting that the directional signal is robust even when the magnitude is small.

2.3.3 Gene-level effects are biologically coherent

At the gene level, feature steering produced biologically interpretable logit changes (Figure 5). The top positive steerer, L5 F4349 (Pre-mRNA Processing), upregulated extracellular matrix genes (ADAMTS2) and developmental regulators. The top negative steerer, L0 F1483 (L-amino Acid Transport), upregulated inflammatory chemokines (CCL3) while downregulating structural proteins. L17 features upregulated transcriptional regulators (KLF9, POLR1E, ZYG11B) consistent with terminal differentiation programs.

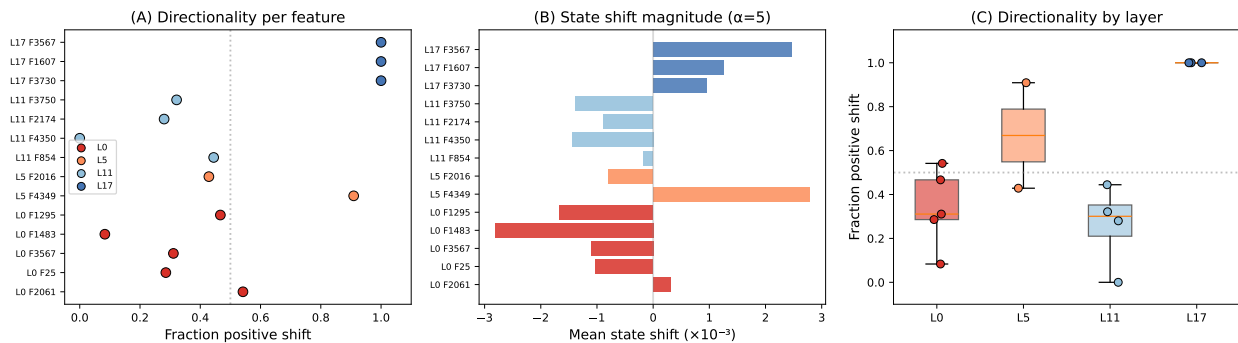


Figure 4: **Trajectory steering directionality.** (A) Fraction of cells showing positive state shift per feature at $\alpha = 5$, colored by layer. L17 features universally push toward maturity (frac. pos. = 1.0); L0 features push away. (B) Mean state shift magnitude at $\alpha = 5$. (C) Box plot of fraction positive grouped by layer, showing that L17 features universally push toward maturity while earlier layers produce mixed or negative shifts.

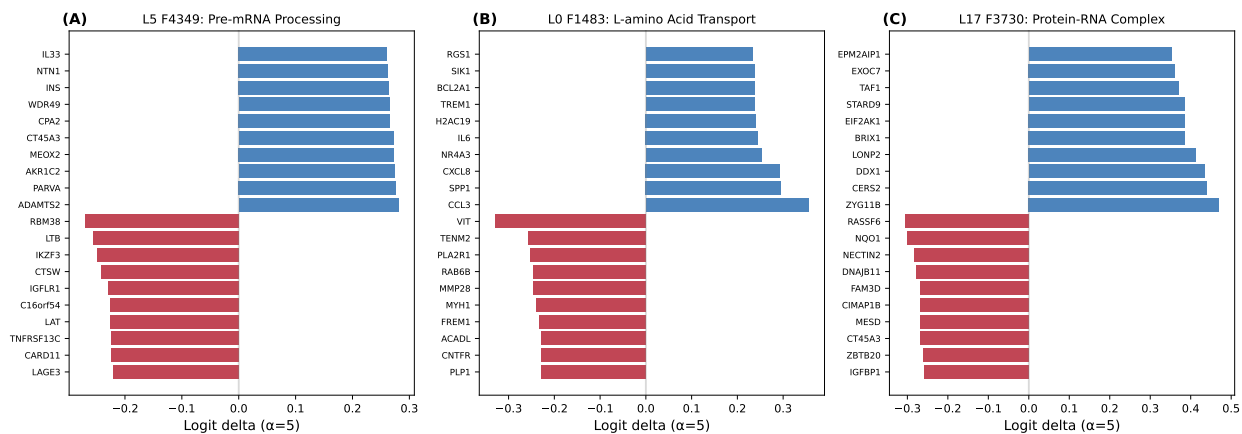


Figure 5: **Gene-level steering effects at $\alpha = 5$.** (A) L5 F4349 (Pre-mRNA Processing): top 10 upregulated and downregulated genes. (B) L0 F1483 (L-amino Acid Transport): top 10 genes. (C) L17 F3730 (Protein-RNA Complex Assembly): top 10 genes.

3 Discussion

These three experiments substantially advance our understanding of how single-cell foundation models organize biological computation, addressing three specific limitations of prior work and revealing unexpected properties of the circuit architecture.

3.1 Annotation bias as a systematic confound

The finding that 40% of the most computationally connected features lack biological annotation is methodologically significant. Interpretability studies that select features based on annotation status [Cunningham et al., 2023, Templeton et al., 2024, Kendiukhov, 2025a] necessarily over-represent well-characterized biology and under-represent novel or poorly characterized computational roles. This parallels concerns in network biology where “study bias”—the tendency to study well-known

Table 4: Trajectory steering results for 14 switch features at $\alpha = 5$. State shift reports the mean change in pseudotime-directed cosine similarity. Frac. pos. is the fraction of steered cells with positive (toward maturity) shift.

Layer	Feature	switch d	Label	Shift ($\times 10^{-3}$)	Frac. pos.	Top gene \uparrow
L0	F2061	1.33	Chromatin Org.	+0.31	0.54	CD24
L0	F25	1.13	Mitotic Spindle	-1.03	0.29	CDCA2
L0	F3567	1.07	<i>unannotated</i>	-1.11	0.31	CLEC4E
L0	F1483	1.07	L-amino Acid	-2.82	0.08	CCL3
L0	F1295	1.01	Neurodegen.	-1.67	0.47	MIIP
L5	F4349	0.95	Pre-mRNA Proc.	+2.79	0.91	ADAMTS2
L5	F2016	0.90	<i>unannotated</i>	-0.80	0.43	MCM4
L11	F854	1.15	RNA Catabolic	-0.17	0.44	UPK1B
L11	F4350	1.09	<i>unannotated</i>	-1.45	0.00	PPP1R14A
L11	F2174	1.01	<i>unannotated</i>	-0.89	0.28	SEMA4F
L11	F3750	1.00	<i>unannotated</i>	-1.39	0.32	C15orf61
L17	F3730	1.25	Prot-RNA Complex	+0.96	1.00	ZYG11B
L17	F1607	1.09	<i>unannotated</i>	+1.25	1.00	POLR1E
L17	F3567	1.09	<i>unannotated</i>	+2.46	1.00	KLF9

genes—distorts interaction databases [Szklarczyk et al., 2023, Gillis et al., 2014]. Exhaustive approaches that do not filter by annotation are essential for unbiased circuit discovery, as demonstrated for language model circuits by Wang et al. [2023], Conmy et al. [2023], and Hanna et al. [2023].

The heavy-tailed hub distribution itself has implications for model robustness: a model with a few thousand features but whose connectivity is concentrated in ~ 70 hub features may be unexpectedly fragile to targeted perturbation of those hubs, while being robust to ablation of the long tail of low-connectivity features. This parallels findings in biological protein networks, where hub proteins are disproportionately essential [Jeong et al., 2001].

3.2 Redundancy as a fundamental design principle

The monotonic deepening of redundancy from single-feature ablation (ratio 1.0) through pairwise (0.74) to three-way (0.59) establishes that Geneformer’s circuit architecture is fundamentally subadditive. This resonates with findings in neural network pruning, where large fractions of parameters can be removed without performance loss [Frankle and Carbin, 2019], suggesting that redundancy is a general property of overparameterized models. The near-zero marginal contribution of a third same-pathway feature (median 0.006–0.184) suggests that most pathway information is already captured by the first two features, with additional features providing diminishing returns—consistent with distributed representations [Hinton, 1986, Olsson et al., 2022] where information is spread across many features but each carries a redundant copy.

The complete absence of synergy at all tested orders is notable. In biological systems, conjunctive regulation—where multiple signals must converge to activate a response—is a common motif in signaling cascades [Alon, 2007]. The lack of synergy in Geneformer suggests that the model does not implement higher-order logical operations across same-pathway features; instead, each feature independently captures a sufficient representation of its pathway’s contribution to downstream computation.

3.3 Layer position encodes differentiation directionality

The causal demonstration that L17 features universally push early cells toward maturity (fraction positive = 1.0) while earlier-layer features (L0, L11) predominantly push them away establishes a functional distinction between late- and early/mid-layer representations. The pattern is not strictly monotonic—L11 features show lower fraction positive (mean 0.26) than L0 features (mean 0.34)—but the L17 endpoint is unambiguous. This is consistent with the progressive refinement hypothesis [Kendiukhov, 2025a]: early and middle layers encode raw gene co-expression patterns (which, when amplified, maintain or disrupt progenitor-like states), while the final layers encode processed cell-identity representations whose amplification drives cells toward terminal differentiation.

This gradient mirrors the biological differentiation hierarchy [Orkin and Zon, 2008, Graf and Enver, 2009], where early transcriptional programs maintain multipotency while late programs commit cells to specific fates. The finding that a transformer model spontaneously learns this hierarchical organization—without explicit supervision on differentiation stage—suggests that the layer-wise processing naturally decomposes cell state into a progression from raw features to commitment signals.

3.4 Scale of the computational graph

The 1,393,850 edges from a single source layer represent a lower bound on the model’s circuit complexity. With 18 layers and $\sim 4,000$ active features per layer, the complete circuit graph would contain on the order of tens of millions of edges. The signal attenuation pattern (L6: 695K \rightarrow L11: 443K \rightarrow L17: 256K) provides a natural compression—distant effects are weaker—but the sheer scale suggests that full circuit analysis of foundation models will require substantial computational investment and novel algorithmic approaches.

3.5 Limitations

Several limitations should be acknowledged. First, exhaustive tracing used only 20 cells per feature (vs. 200 in selective tracing), which reduces statistical power for detecting small effects and may explain the lower mean edges per feature (343 vs. 1,737 in selective tracing). Second, only 3 downstream layers were measured (L6, L11, L17) versus 12 in selective tracing, meaning intermediate-layer effects are not captured. Third, the three-way ablation tested only 8 triplets across 4 pathways; while results were consistent, broader coverage would strengthen the generalizability claim. Fourth, trajectory steering effects were small in absolute magnitude (~ 0.001 – 0.003), raising questions about biological significance despite directional consistency. Fifth, all experiments were conducted on Geneformer only; replication in other foundation models (scGPT [Cui et al., 2024], scBERT [Yang et al., 2022]) and in protein foundation models [Rives et al., 2021] would test whether these architectural properties are model-specific or universal.

3.6 Conclusions

The transition from selective to exhaustive circuit analysis reveals that the “map” drawn by annotation-biased sampling systematically misrepresents the territory. The complete L5 circuit graph is dominated by unannotated hub features, organized in a heavy-tailed distribution, and characterized by deep redundancy without synergy. Combined with the causal evidence that late-layer (L17) features uniquely and universally drive cell state toward maturity while earlier layers do not, these results establish that Geneformer’s internal representations encode a biologically

meaningful functional specialization—implemented through massively redundant, hub-dominated circuits.

4 Methods

4.1 Model and sparse autoencoders

All experiments used Geneformer V2-316M [Theodoris et al., 2023], an 18-layer, 18-head transformer model pre-trained on ~ 100 million single-cell transcriptomes. TopK sparse autoencoders [Makhzani and Frey, 2013] ($k = 32$, $4\times$ overcomplete: $d_{\text{model}} = 1,152 \rightarrow d_{\text{SAE}} = 4,608$) were trained on residual stream [Elhage et al., 2022] activations at each layer using 4.05 million token positions from K562 cells, as described in Kendiukhov [2025b]. Features were annotated by computing cosine similarity between decoder directions and gene embedding vectors, selecting the top 50 loading genes per feature, and performing enrichment analysis [Subramanian et al., 2005] against GO [Ashburner et al., 2000], KEGG [Kanehisa and Goto, 2000], and Reactome [Jassal et al., 2020] databases.

4.2 Exhaustive circuit tracing

For each of the 4,065 features at layer 5 with activation frequency ≥ 0.001 , we performed causal ablation tracing [Pearl, 2009, Vig et al., 2020, Geiger et al., 2021] across 20 randomly sampled K562 cells. A clean forward pass cache was pre-computed once, storing source-layer hidden states, SAE encodings, and downstream clean SAE activations for all cells—a critical optimization that eliminated redundant forward passes, reducing computation from ~ 20 days to 17.7 hours. For each feature, we set its TopK activation coefficient to zero in the source-layer residual stream, ran a forward pass from that layer, and encoded the downstream hidden states through the corresponding layer SAEs. Cohen’s d between clean and ablated activations was computed using Welford’s online accumulator [Welford, 1962]. Edges with $|d| > 0.5$ and consistency > 0.7 were retained as significant. Three downstream layers (6, 11, 17) were measured. Total compute time was 17.7 hours on a single Apple M2 Max GPU (MPS backend).

4.3 Higher-order combinatorial ablation

Eight feature triplets were constructed across four biological pathways (vesicle transport: 3 triplets; mitosis: 2; metabolism: 2; cross-pathway DDR \times mitosis: 1), each containing features from layers 0, 5, and 11 with the same or related GO/pathway annotations. For each triplet, 7 ablation conditions were tested (A, B, C, AB, AC, BC, ABC) plus a clean baseline, with 200 K562 cells per condition. The three-way redundancy ratio was computed as:

$$R_{ABC} = \frac{|d_{ABC}|}{|d_A| + |d_B| + |d_C|}$$

The higher-order interaction term was computed via inclusion-exclusion:

$$I_{ABC} = d_{ABC} - d_{AB} - d_{AC} - d_{BC} + d_A + d_B + d_C$$

A target was classified as superadditive if $|d_{ABC}| > |d_A| + |d_B| + |d_C|$ (i.e., $R_{ABC} > 1$). Total compute time was 6.5 hours.

4.4 Trajectory-guided feature steering

Fourteen switch features identified in Kendiukhov [2025a] were selected for steering: 5 from L0, 2 from L5, 4 from L11, and 3 from L17. For each feature, we identified early-pseudotime cells (bottom 30% of diffusion pseudotime [Haghverdi et al., 2016]) from 481 Tabula Sapiens [The Tabula Sapiens Consortium, 2022] immune cells, where the feature was active. Steering was performed following the activation addition framework [Turner et al., 2023, Li et al., 2024], by multiplying the feature’s SAE activation coefficient by $\alpha \in \{2.0, 5.0\}$ and reconstructing the modified residual stream:

$$h'_\ell = h_\ell + (\alpha - 1) \cdot a_f \cdot d_f$$

where a_f is the activation coefficient and d_f is the decoder direction for feature f . The modified hidden state was then propagated through the remaining model layers to obtain logit changes.

State shift was quantified as:

$$\Delta s = \cos(z', g_{\text{late}}) - \cos(z', g_{\text{early}}) - [\cos(z, g_{\text{late}}) - \cos(z, g_{\text{early}})]$$

where z and z' are the clean and steered logit vectors, and $g_{\text{late}}, g_{\text{early}}$ are gene expression signatures computed from the top and bottom pseudotime deciles. Positive Δs indicates a shift toward maturity. Total compute time was 2.1 minutes.

4.5 Reproducibility

All code is available at <https://github.com/Biodyn-AI/sae-biological-map>. Experiments were run on a MacBook Pro with Apple M2 Max (38-core GPU, 96 GB unified memory) using PyTorch 2.1 with MPS backend. Python environment: conda with NumPy 1.26.4, scanpy [Wolf et al., 2018]. Total compute time for all experiments reported in this paper: ~ 26.3 hours. Random seeds were fixed for reproducibility.

Data Availability

The datasets analysed during the current study are available in the following repositories:

- **K562 CRISPRi perturbation data** (Replogle et al. [Replogle et al., 2022]): available at https://plus.figshare.com/articles/dataset/Replogle_2022_K562_gwps/21452470 (Figshare, DOI: 10.6084/m9.figshare.21452470).
- **Tabula Sapiens** single-cell atlas [The Tabula Sapiens Consortium, 2022]: available at <https://tabula-sapiens-portal.ds.czbiohub.org/> and via CZ CELLxGENE (<https://cellxgene.cziscience.com/collections/e5f58829-1a66-40b5-a624-9046778e74f5>).
- **Geneformer V2-316M** pretrained model [Theodoris et al., 2023]: available on HuggingFace at <https://huggingface.co/ctheodoris/Geneformer> (subfolder `Geneformer-V2-316M`).
- **Gene Ontology** annotations [Ashburner et al., 2000]: available at <http://geneontology.org/>.

All derived experimental data (trained SAE weights, feature catalogs, circuit graphs, and analysis outputs) are available at <https://github.com/Biodyn-AI/sae-biological-map>.

Code Availability

All code for SAE training, feature analysis, causal patching, circuit tracing, and figure generation is available at <https://github.com/Biodyn-AI/sae-biological-map>.

Author Contributions

I.K. conceived the study, designed and performed all experiments, analyzed the results, and wrote the manuscript.

Funding

This work was self-funded by the author.

Competing Interests

The author declares no competing interests.

Acknowledgments

The author thanks the developers of Geneformer, scanpy, and PyTorch for making their software freely available.

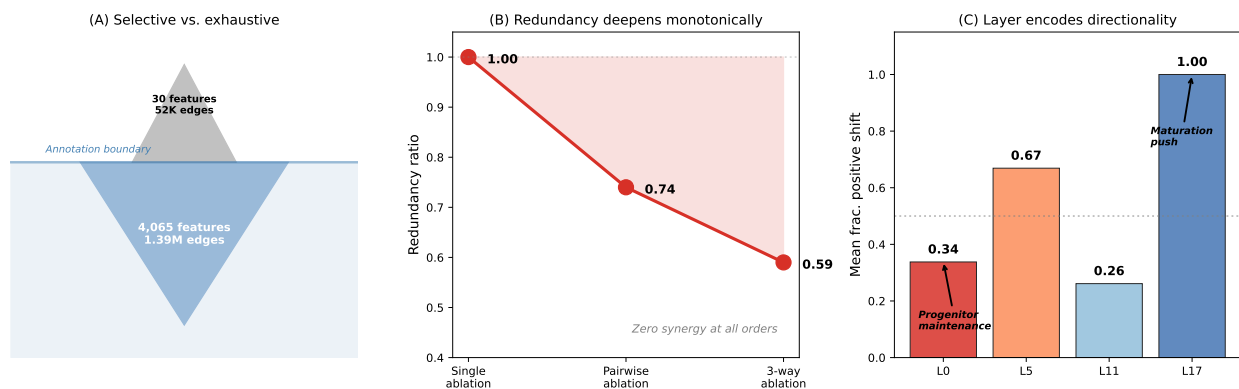


Figure 6: **Summary of findings.** (A) Selective tracing reveals only the “tip of the iceberg”; exhaustive tracing exposes the full circuit graph including unannotated hub features. (B) Redundancy ratio decreases from single (1.0) to pairwise (0.74) to three-way (0.59) ablation, with zero synergy at all orders. (C) Layer position encodes steering directionality: early-layer features produce mixed or negative shifts, while L17 features universally drive maturation.

References

Réka Albert and Albert-László Barabási. Statistical mechanics of complex networks. *Reviews of Modern Physics*, 74(1):47–97, 2002.

- Uri Alon. Network motifs: theory and experimental approaches. *Nature Reviews Genetics*, 8(6): 450–461, 2007.
- Michael Ashburner, Catherine A Ball, Judith A Blake, David Botstein, Heather Butler, J Michael Cherry, Allan P Davis, Kara Dolinski, Selina S Dwight, Janan T Eppig, et al. Gene Ontology: tool for the unification of biology. *Nature Genetics*, 25(1):25–29, 2000.
- Albert-László Barabási and Réka Albert. Emergence of scaling in random networks. *Science*, 286(5439):509–512, 1999.
- Albert-László Barabási and Zoltán N. Oltvai. Network biology: understanding the cell’s functional organization. *Nature Reviews Genetics*, 5(2):101–113, 2004.
- Leonard Bereska and Efstratios Gavves. Mechanistic interpretability for AI safety—a review. *arXiv preprint arXiv:2404.14082*, 2024.
- Trenton Bricken, Adly Templeton, Joshua Batson, Brian Chen, Adam Jermyn, Tom Conerly, Nick Turner, Cem Anil, Carson Denison, Amanda Askell, et al. Towards monosemanticity: Decomposing language models with dictionary learning. *Transformer Circuits Thread*, 2023.
- Navdeep S. Chandel. Mitochondria. *Cold Spring Harbor Perspectives in Biology*, 13(3):a040543, 2021.
- Alberto Ciccia and Stephen J. Elledge. The DNA damage response: making it safe to play with knives. *Molecular Cell*, 40(2):179–204, 2010.
- Jacob Cohen. *Statistical Power Analysis for the Behavioral Sciences*. Lawrence Erlbaum Associates, 2nd edition, 1988.
- Arthur Conmy, Augustine N. Mavor-Parker, Aengus Lynch, Stefan Heimersheim, and Adrià Garriga-Alonso. Towards automated circuit discovery for mechanistic interpretability. In *Advances in Neural Information Processing Systems*, volume 36, 2023.
- Haotian Cui, Chloe Wang, Hassaan Maan, Kuan Pang, Fengning Luo, Nan Duan, and Bo Wang. scGPT: toward building a foundation model for single-cell multi-omics using generative AI. *Nature Methods*, 21(8):1470–1480, 2024.
- Hoagy Cunningham, Aidan Ewart, Logan Riggs, Robert Huben, and Lee Sharkey. Sparse autoencoders find highly interpretable features in language models. *arXiv preprint arXiv:2309.08600*, 2023.
- Jacob Devlin, Ming-Wei Chang, Kenton Lee, and Kristina Toutanova. BERT: Pre-training of deep bidirectional transformers for language understanding. In *Proceedings of the 2019 Conference of the North American Chapter of the Association for Computational Linguistics: Human Language Technologies*, pages 4171–4186, 2019.
- Nelson Elhage, Tristan Hume, Catherine Olsson, Nicholas Schiefer, Tom Henighan, Shaul Kravec, Zac Hatfield-Dodds, Robert Lasenby, Dawn Drain, Carol Chen, et al. Toy models of superposition. *Transformer Circuits Thread*, 2022.
- Jonathan Frankle and Michael Carbin. The lottery ticket hypothesis: Finding sparse, trainable neural networks. In *International Conference on Learning Representations*, 2019.

- Leo Gao, Tom Dupré la Tour, Henk Tillman, Gabriel Goh, Rajan Troll, Alec Radford, Ilya Sutskever, Jan Leike, and Jeff Wu. Scaling and evaluating sparse autoencoders. *arXiv preprint arXiv:2406.04093*, 2024.
- Atticus Geiger, Hanson Lu, Thomas Icard, and Christopher Potts. Causal abstractions of neural networks. *Advances in Neural Information Processing Systems*, 34:9574–9586, 2021.
- Jesse Gillis, Sara Ballouz, Prashant Bhatt, and Paul Pavlidis. Bias tradeoffs in the creation and analysis of protein–protein interaction networks. *Journal of Proteomics*, 100:44–54, 2014.
- Thomas Graf and Tariq Enver. Forcing cells to change lineages. *Nature*, 462(7273):587–594, 2009.
- Laleh Haghverdi, Maren Büttner, F Alexander Wolf, Florian Buettner, and Fabian J Theis. Diffusion pseudotime robustly reconstructs lineage branching. *Nature Methods*, 13(10):845–848, 2016.
- Michael Hanna, Ollie Liu, and Alexandre Variengien. How does GPT-2 compute greater-than?: Interpreting mathematical abilities in a pre-trained language model. In *Advances in Neural Information Processing Systems*, volume 36, 2023.
- Minsheng Hao, Jing Gong, Xin Zeng, Chiming Liu, Yucheng Guo, Xingyi Cheng, Taifeng Wang, Jianzhu Ma, Xuegong Zhang, and Le Song. Large scale foundation model on single-cell transcriptomics. *Nature Methods*, 21(8):1481–1491, 2024.
- Kaiming He, Xiangyu Zhang, Shaoqing Ren, and Jian Sun. Deep residual learning for image recognition. In *Proceedings of the IEEE Conference on Computer Vision and Pattern Recognition*, pages 770–778, 2016.
- Geoffrey E. Hinton. Distributed representations. *Parallel Distributed Processing: Explorations in the Microstructure of Cognition*, 1:77–109, 1986.
- Stephen P. Jackson and Jiri Bartek. The DNA-damage response in human biology and disease. *Nature*, 461(7267):1071–1078, 2009.
- Bijay Jassal, Lisa Matthews, Guilherme Viteri, Chuqiao Gong, Pascual Lorente, Antonio Fabregat, Konstantinos Sidiropoulos, Justin Cook, Marc Gillespie, Robin Haw, et al. The Reactome pathway knowledgebase. *Nucleic Acids Research*, 48(D1):D498–D503, 2020.
- Hawoong Jeong, Sean P. Mason, Albert-László Barabási, and Zoltán N. Oltvai. Lethality and centrality in protein networks. *Nature*, 411(6833):41–42, 2001.
- Minoru Kanehisa and Susumu Goto. KEGG: Kyoto Encyclopedia of Genes and Genomes. *Nucleic Acids Research*, 28(1):27–30, 2000.
- Ihor Kendiukhov. Causal circuit tracing reveals distinct computational architectures in a single-cell foundation model. *arXiv preprint*, 2025a. Companion paper.
- Ihor Kendiukhov. Sparse autoencoders reveal organized biological knowledge but minimal regulatory logic in single-cell foundation models: A comparative atlas of Geneformer and scGPT. *arXiv preprint*, 2025b. Companion paper.
- Ihor Kendiukhov. Systematic evaluation of single-cell foundation model interpretability reveals attention captures co-expression rather than unique regulatory signal. *arXiv preprint*, 2025c. Companion paper.

- Kenneth Li, Oam Patel, Fernanda Viégas, Hanspeter Pfister, and Martin Wattenberg. Inference-time intervention: Eliciting truthful answers from a language model. *Advances in Neural Information Processing Systems*, 36, 2024.
- Alireza Makhzani and Brendan J Frey. k-sparse autoencoders. *arXiv preprint arXiv:1312.5663*, 2013.
- Marcos Malumbres and Mariano Barbacid. Cell cycle, CDKs and cancer: a changing paradigm. *Nature Reviews Cancer*, 9(3):153–166, 2009.
- Samuel Marks, Can Rager, Eric J. Michaud, Yonatan Belinkov, David Bau, and Aaron Mueller. Sparse feature circuits: Discovering and editing interpretable causal graphs in language models. *arXiv preprint arXiv:2403.19647*, 2024.
- Kevin Meng, David Bau, Alex Andonian, and Yonatan Belinkov. Locating and editing factual associations in GPT. *Advances in Neural Information Processing Systems*, 35:17359–17372, 2022.
- Andrea Musacchio and Edward D. Salmon. The spindle-assembly checkpoint in space and time. *Nature Reviews Molecular Cell Biology*, 8(5):379–393, 2007.
- Chris Olah, Nick Cammarata, Ludwig Schubert, Gabriel Goh, Michael Petrov, and Shan Carter. Zoom in: An introduction to circuits. *Distill*, 2020. <https://distill.pub/2020/circuits/zoom-in/>.
- Catherine Olsson, Nelson Elhage, Neel Nanda, Nicholas Joseph, Nova DasSarma, Tom Henighan, Ben Mann, Amanda Askell, Yuntao Bai, Anna Chen, et al. In-context learning and induction heads. *Transformer Circuits Thread*, 2022.
- Stuart H. Orkin and Leonard I. Zon. Hematopoiesis: an evolving paradigm for stem cell biology. *Cell*, 132(4):631–644, 2008.
- Judea Pearl. *Causality: Models, Reasoning, and Inference*. Cambridge University Press, 2nd edition, 2009.
- Aviv Regev, Sarah A Teichmann, Eric S Lander, Ido Amit, Christophe Benoist, Ewan Birney, Bernd Bodenmiller, Peter Campbell, Piero Carninci, Menna Clatworthy, et al. The Human Cell Atlas. *eLife*, 6:e27041, 2017.
- Joseph M Repogle, Reuben A Saunders, Alexandra N Pogson, Jeffrey A Hussmann, Alexander Lenail, Alina Guna, Lauren Mascibroda, Eric J Wagner, Karen Adelman, Gila Lithwick-Yanai, et al. Mapping information-rich genotype-phenotype landscapes with genome-scale Perturb-seq. *Cell*, 185(14):2559–2575, 2022.
- Alexander Rives, Joshua Meier, Tom Sercu, Siddharth Goyal, Zeming Lin, Jason Liu, Demi Guo, Myle Ott, C Lawrence Zitnick, Jerry Ma, and Rob Fergus. Biological structure and function emerge from scaling unsupervised learning to 250 million protein sequences. *Proceedings of the National Academy of Sciences*, 118(15):e2016239118, 2021.
- Lee Sharkey, Dan Braun, and Beren Millidge. Taking features out of superposition with sparse autoencoders. *Alignment Forum*, 2022.
- Kai Simons and Elina Ikonen. How cells handle cholesterol. *Science*, 290(5497):1721–1726, 2000.

- Aravind Subramanian, Pablo Tamayo, Vamsi K Mootha, Sayan Mukherjee, Benjamin L Ebert, Michael A Gillette, Amanda Paulovich, Scott L Pomeroy, Todd R Golub, Eric S Lander, and Jill P Mesirov. Gene set enrichment analysis: A knowledge-based approach for interpreting genome-wide expression profiles. *Proceedings of the National Academy of Sciences*, 102(43):15545–15550, 2005.
- Damian Szklarczyk, Rebecca Kirsch, Mikaela Koutrouli, Katerina Nastou, Farrokh Mehryary, Radja Hachilif, Annika L Gable, Tao Fang, Nadezhda T Doncheva, Sampo Pyysalo, et al. The STRING database in 2023: protein–protein association networks and functional enrichment analyses for any sequenced genome of interest. *Nucleic Acids Research*, 51(D1):D638–D646, 2023.
- Adly Templeton, Tom Conerly, Jonathan Marcus, Jack Lindsey, Trenton Bricken, Brian Chen, Adam Pearce, Craig Citro, Emmanuel Ameisen, Andy Jones, et al. Scaling monosemanticity: Extracting interpretable features from Claude 3 Sonnet. *Transformer Circuits Thread*, 2024.
- The Tabula Sapiens Consortium. The Tabula Sapiens: A multiple-organ, single-cell transcriptomic atlas of humans. *Science*, 376(6594):eabl4896, 2022.
- Christina V Theodoris, Ling Xiao, Anant Chopra, Mark D Chaffin, Zeina R Al Sayed, Matthew C Hill, Helene Manber, Jesse M Engreitz, et al. Transfer learning enables predictions in network biology. *Nature*, 618(7965):616–624, 2023.
- Cole Trapnell, Davide Cacchiarelli, Jonna Grimsby, Prapti Pokharel, Shuqiang Li, Michael Morse, Niall J Lennon, Kenneth J Livak, Tarjei S Mikkelsen, and John L Rinn. The dynamics and regulators of cell fate decisions are revealed by pseudotemporal ordering of single cells. *Nature Biotechnology*, 32(4):381–386, 2014.
- Alexander Matt Turner, Lisa Thiergart, David Udell, Gavin Leech, Ulisse Mini, and Monte Pieler. Activation addition: Steering language models without optimization. *arXiv preprint arXiv:2308.10248*, 2023.
- Ashish Vaswani, Noam Shazeer, Niki Parmar, Jakob Uszkoreit, Llion Jones, Aidan N Gomez, Łukasz Kaiser, and Illia Polosukhin. Attention is all you need. In *Advances in Neural Information Processing Systems*, volume 30, pages 5998–6008, 2017.
- Jesse Vig, Sebastian Gehrmann, Yonatan Belinkov, Sharon Qian, Daniel Nevo, Simas Sakenis, Jason Huang, Yaron Singer, and Stuart Shieber. Causal mediation analysis for interpreting neural NLP: The case of gender bias. *arXiv preprint arXiv:2004.12265*, 2020.
- Kevin Wang, Alexandre Variengien, Arthur Conmy, Buck Shlegeris, and Jacob Steinhardt. Interpretability in the wild: a circuit for indirect object identification in GPT-2 small. In *International Conference on Learning Representations*, 2023.
- B. P. Welford. Note on a method for calculating corrected sums of squares and products. *Technometrics*, 4(3):419–420, 1962.
- F Alexander Wolf, Philipp Angerer, and Fabian J Theis. SCANPY: large-scale single-cell gene expression data analysis. *Genome Biology*, 19(1):15, 2018.
- F Alexander Wolf, Fiona K Hamey, Mireya Plass, Jordi Solana, Joakim S Dahlin, Berthold Göttgens, Nikolaus Rajewsky, Lukas Simon, and Fabian J Theis. PAGA: graph abstraction reconciles clustering with trajectory inference through a topology preserving map of single cells. *Genome Biology*, 20(1):59, 2019.

- Fan Yang, Wenchuan Wang, Fang Wang, Yuan Fang, Duyu Tang, Junzhou Huang, Hui Lu, and Jianhua Yao. scBERT as a large-scale pretrained deep language model for cell type annotation of single-cell RNA-seq data. *Nature Machine Intelligence*, 4(10):852–866, 2022.
- Grace X Y Zheng, Jessica M Terry, Phillip Belgrader, Paul Ryvkin, Zachary W Bent, Ryan Wilson, Solongo B Ziraldo, Tobias D Wheeler, Geoff P McDermott, Junjie Zhu, et al. Massively parallel digital transcriptional profiling of single cells. *Nature Communications*, 8:14049, 2017.
- Andy Zou, Long Phan, Sarah Chen, James Campbell, Phillip Guo, Richard Ren, Alexander Pan, Xuwang Yin, Mantas Mazeika, Ann-Kathrin Dombrowski, et al. Representation engineering: A top-down approach to AI transparency. *arXiv preprint arXiv:2310.01405*, 2023.